LASER INTERFEROMETER GRAVITATIONAL WAVE OBSERVATORY
- LIGO -
CALIFORNIA INSTITUTE OF TECHNOLOGY
MASSACHUSETTS INSTITUTE OF TECHNOLOGY

Technical Note	**LIGO-T2400223–v1**	2024/07/18

First Interim SURF Report

Erin Coleman

Distribution of this document:

AIC, ISC

California Institute of Technology
LIGO Project, MS 18-34
Pasadena, CA 91125
Phone (626) 395-2129
Fax (626) 304-9834
E-mail: info@ligo.caltech.edu

Massachusetts Institute of Technology
LIGO Project, Room NW22-295
Cambridge, MA 02139
Phone (617) 253-4824
Fax (617) 253-7014
E-mail: info@ligo.mit.edu

LIGO Hanford Observatory
Route 10, Mile Marker 2
Richland, WA 99352
Phone (509) 372-8106
Fax (509) 372-8137
E-mail: info@ligo.caltech.edu

LIGO Livingston Observatory
19100 LIGO Lane
Livingston, LA 70754
Phone (225) 686-3100
Fax (225) 686-7189
E-mail: info@ligo.caltech.edu

http://www.ligo.caltech.edu/

1 Introduction

Gravitational waves (GWs) are perturbations in spacetime caused by compact objects moving at relativistic speeds. They are now routinely observed with interferometry by GW observatories around the world [1]. One major source of GWs is binary black hole (BH) mergers. The final stage of a BH merger is known as the ringdown.

The ringdown occurs because a BH merger results in a single perturbed BH. This perturbed BH radiates gravitational energy to settle into a more stable state. The ringdown can be decomposed into quasinormal modes (QNMs) indexed with indices (ℓ, m, n). Each QNM has angular dependence given by spin-weighted spheroidal harmonics and a complex frequency $\omega_{\ell mn} = 2\pi f_{\ell mn} - i/\tau_{\ell mn}$. These modes are called QNMs because, unlike normal modes, they decay over time. The real component of $\omega_{\ell mn}$ indicates the oscillatory frequency of that particular mode, and the imaginary component indicates how quickly it decays [2, 3, 4].

Within general relativity GWs have two possible polarizations, denoted by h_+ and $h_\times$. It is convenient to describe the overall strain in both polarizations as a complex number $h = h_+ - ih_\times$. Setting the ringdown start time $t_0 = 0$, the overall ringdown waveform at time $t > 0$ is given by the equation

$$h(t, \theta, \varphi) = h_+(t, \theta, \varphi) - ih_\times(t, \theta, \varphi) = \sum_{\ell=2}^{\infty} \sum_{m=-\ell}^{\ell} \sum_{n=0}^{\infty} {}_{-2}S_{\ell mn}(\theta, \varphi) C_{\ell mn} e^{-i\omega_{\ell mn} t} \tag{1}$$

where ${}_{-2}S_{\ell mn}$ are the spheroidal harmonic functions and $C_{\ell mn} = A_{\ell mn} e^{i\phi_{\ell mn}}$ is a complex amplitude. In the coordinate system typically used by numerical relativity (NR) simulations, the binary BHs are initially along the x axis, orbiting one another in the x-y plane, and the z-axis points in the direction of the initial orbital angular momentum vector. The angles θ and φ represent the polar and azimuthal angles in this frame, as in the typical formulation of spherical coordinates. This project will focus on the amplitudes $C_{\ell mn}$.

However, in NR, h is written as a sum of modes

$$h = \sum_{\ell=2}^{\infty} \sum_{m=-\ell}^{\ell} h_{\ell m}(t) {}_{-2}Y_{\ell m}(\theta, \varphi) \tag{2}$$

over the spin-weighted spherical harmonics ${}_{-2}Y_{\ell m}$ instead of the spheroidal harmonics ${}_{-2}S_{\ell mn}$. In this basis, every spherical harmonic mode has contributions from every QNM of the same m. This is an effect known as mode mixing.

If a QNM can be recovered from a real GW signal, the resultant final BH mass M_f and dimensionless spin χ_f can be calculated. The No-Hair Theorem, which is a significant theorem in general relativity, states that these properties are the only properties of an astrophysical BH [4]. Thus, measuring the amplitudes of different QNMs in a GW from a binary BH merger is an important test of general relativity. This technique is known as black hole spectroscopy [5]. We can measure the frequencies of all QNMs received, and determine whether they are consistent with a single value of χ_f and M_f. We can study the ringdown of NR waveforms to inform our analysis of real GW data.

Recent studies have focused on fitting the amplitudes of the overtones of the $(2, 2)$ mode, which dominates the waveform. The overtones are tones with $n \geq 1$. Giesler et al. found

that overtones up to $n = 7$ could be fit to the waveform, stretching back to the time of peak strain [3]. However, the same study found that the overtone amplitudes did not decay as expected when fitting the ringdown at different times. A more careful approach is required. A more recent study by Clarke et al. fit QNM overtone amplitudes using Bayesian analysis to classify tone amplitudes as stably recovered, unstably recovered, or unresolved depending on the consistency of the amplitude and phase of the recovered tone with subsequent fits [2].

2 Progress

In the first part of this project, I have studied least-squares fits of the ringdown of binary black hole (BBH) mergers. In particular, we have investigated the effects of fitting different numbers of overtones of the fundamental $(2, 2, 0)$ mode. So far, we have run fits on the dominant $\ell = m = 2$ spherical harmonic mode of a set of CCE simulated waveforms for BBH mergers with spins aligned along the z axis. We will be working with the aligned-spin CCE waveforms available in the SXS catalog [6, 7]. These were mapped to the remnant ("superrest") frame via the `scri` [8] Python package.

2.1 Mismatch studies

We are studying the "usefulness" of adding additional overtones to a fit. One measure of usefulness is the additional signal time which can be used in a fit. Fitting additional overtones allows the signal to be a good fit earlier. This is desirable because the amplitudes of QNMs decay exponentially, so earlier times have a higher signal to noise ratio.

Let $t_0^{N,\mathcal{M}}$ be the earliest time at which a fit with N overtones in addition to the fundamental mode is a good fit, as quantified by the mismatch. To determine $t_0^{N,\mathcal{M}}$ for a particular signal, we generated a mismatch curve for the signal. The mismatch $\mathcal{M}$ between two signals h_1 and h_2 is defined to be

$$\mathcal{M} = 1 - \frac{\langle h_1|h_2\rangle}{\sqrt{\langle h_1|h_1\rangle\langle h_2|h_2\rangle}}$$

where the inner product $\langle h_1|h_2\rangle$ is defined as

$$\langle h_1|h_2\rangle = \mathrm{Re}\left[\int_{t_0}^{T} h_1(t)h_2^*(t)\mathrm{d}t\right] \tag{3}$$

and t_0 and T are the start and end times of the two signals. In the mismatch curve, we plotted $\mathcal{M}$ vs t_0 with $T = t_0 + 100M$ for $N = 0$ through $N = 21$. Beyond $N = 21$, it becomes difficult to calculate QNM frequencies, but as will be detailed later, 21 overtones is sufficient. We used the knee-finding Python package `kneed` [9, 10] to find the knee of the mismatch curve for each fit. This is the value of t_0 at which the mismatch curve begins to increase rapidly, which means that it is the earliest time at which a fit with N overtones is a good fit. Thus, each knee is at $t_0^{N,\mathcal{M}}$. Figure 1 shows the mismatch curve for CCE waveform `SXS_BBH_ExtCCE_0001` (CCE1). Note that although $t_0^{N,\mathcal{M}}$ is the earliest time at which a fit with N overtones is a good fit, that fit is not necessarily physical. For early enough values of t, the GW signal is from the BH merger, not the ringdown, so ringdown models should not be applied.

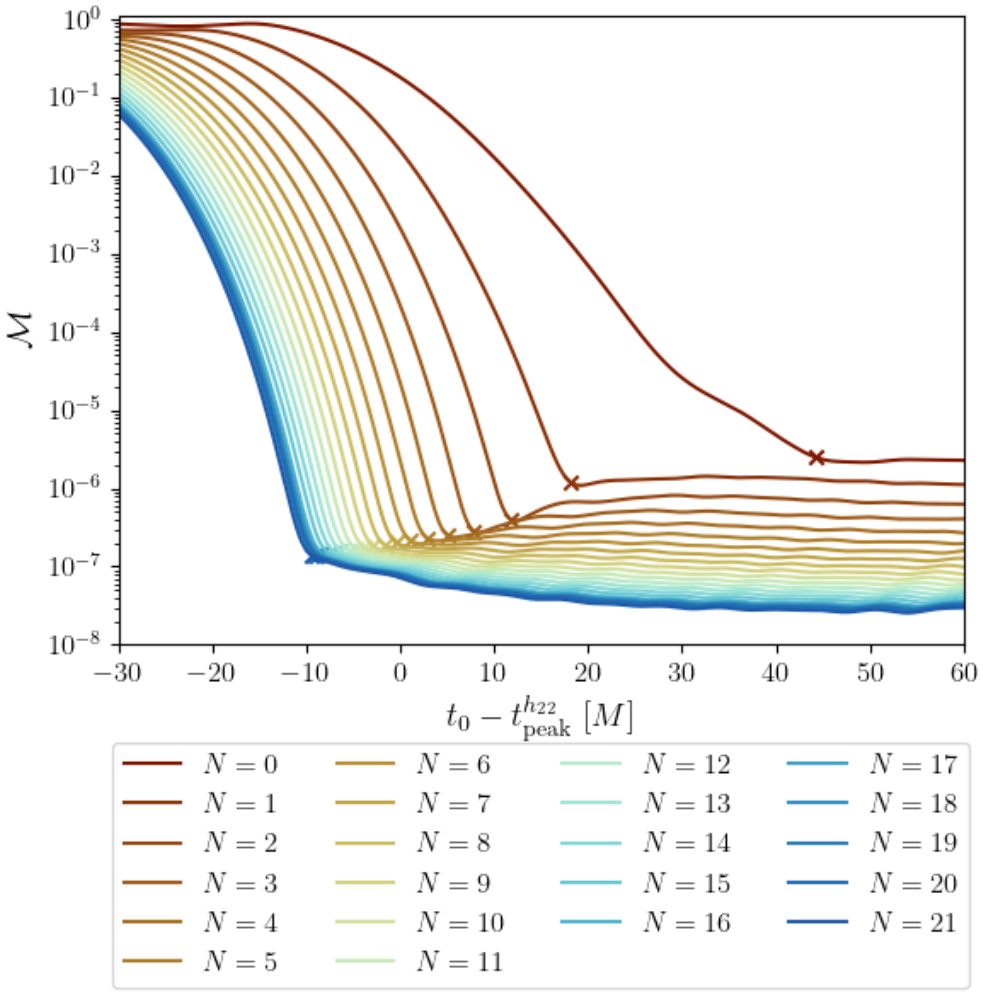

Figure 1: The mismatch curve for CCE1 for fits of 0 through 21 overtones of the $(2, 2)$ mode. Crosses mark the location of $t_0^{N,\mathcal{M}}$ for each N value.

We have defined one measure of usefulness to be the difference $\Delta t_0^{N,\mathcal{M}} = t_0^{N,\mathcal{M}} - t_0^{N-1,\mathcal{M}}$. Note that $\Delta t_0^{N,\mathcal{M}}$ is not defined for $N < 1$. This is a measure of how much additional signal can be fitted by adding the Nth overtone. It should always be positive, because more overtones will fit a signal better, and allow the signal to be fitted at earlier times. Figure 2 shows $\Delta t_0^{N,\mathcal{M}}$ as a function of N for ten CCE waveforms. As expected, for all waveforms studied, $\Delta t_0^{N,\mathcal{M}}$ decreases rapidly toward zero. However, at $N = 18$, every waveform studied had $\Delta t_0^{N,\mathcal{M}} < 0$. This was unexpected, because every additional overtone should extend the fit to earlier times. This suggests that at $N = 18$ overtones, we begin to run up against the limit of the NR simulation precision, and that the maximum usable number of overtones is 17.

We are interested in the location of the "knees" in Figure 1. We do not yet understand why the mismatch levels out at a value of approximately $\mathcal{M} = 10^{-6}$ for times after $t_0^{N,\mathcal{M}}$. To try to investigate this phenomenon further, we created an injection waveform.

Because the ringdown is made up of spheroidal harmonics, each spherical harmonic mode has

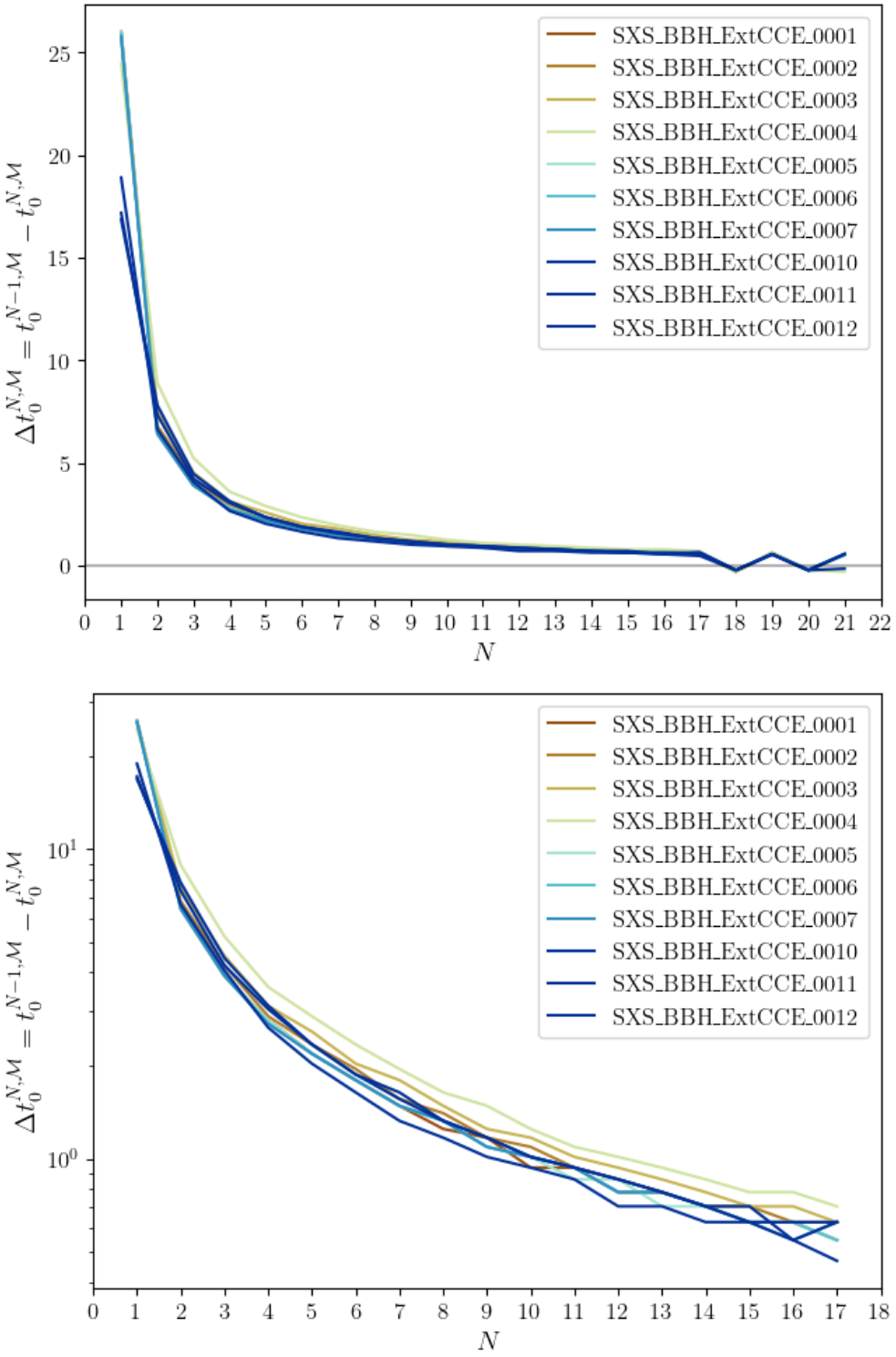

Figure 2: $\Delta t_0^{N,\mathcal{M}}$ vs N for ten different CCE waveforms. The upper panel shows the plot on a linear scale for $N \in [1, 21]$, and the lower panel shows the plot on a logarithmic scale for $N \in [1, 17]$.

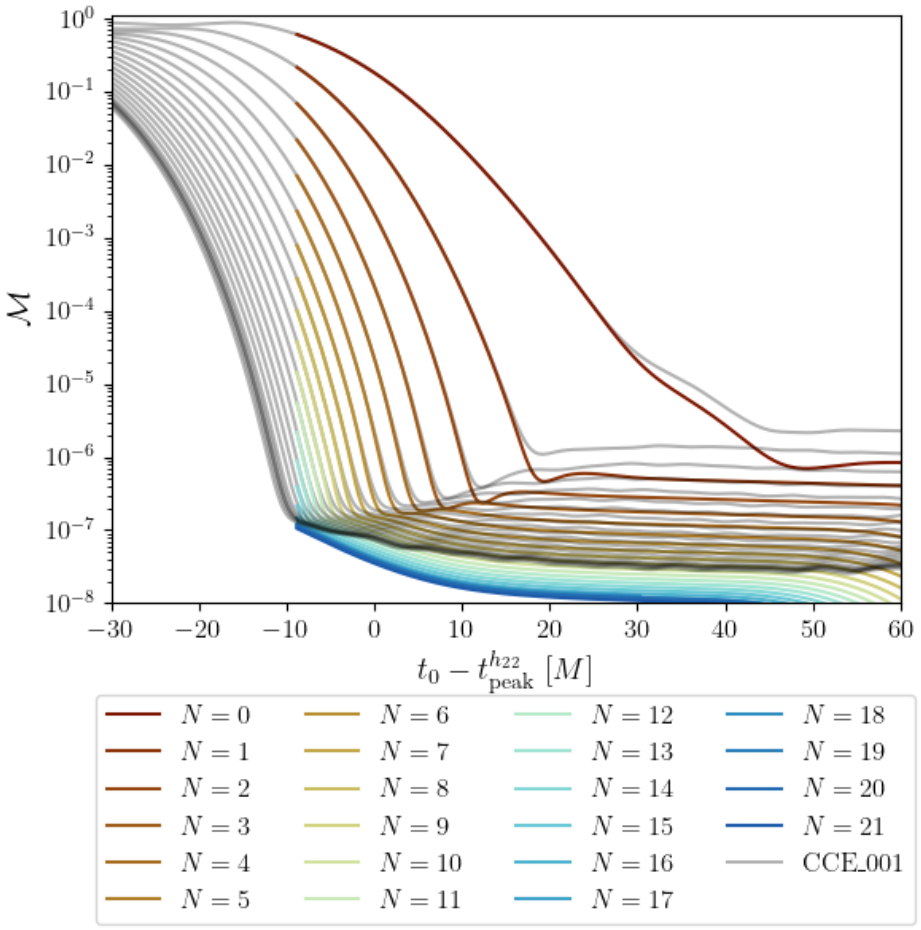

Figure 3: A plot of the mismatch between the injection waveform for fits of 0 through 20 overtones of the $(2, 2, 0)$ QNM. The gray lines show the mismatch curves in Figure 1.

contributions from all other QNMs of the same m. The QNM with the largest contribution to the $(2, 2, 0)$ mode is the $(3, 2, 0)$ mode. We fitted CCE1 with the QNMs $(2, 2, 0)$ through $(2, 2, 17)$ and $(3, 2, 0)$ at $t_0 = t_0^{17,\mathcal{M}}$. Then, we created a pure waveform using the fitted amplitudes of each mode, with the sum

$$h_{\rm I}(t) = \left(\sum_{n=0}^{17} A_{22n} e^{-i\omega_{22n}(t-t_0)} \right) + A_{320} e^{-i\omega_{320}(t-t_0)}.$$

We then fitted this waveform to a model containing up to $N = 20$ overtones of the $(2, 2, 0)$ QNM, without including the $(3, 2, 0)$ QNM in the model.

As shown in Figure 3, we were able to reproduce the knee behavior seen in Figure 1. When we fitted the injection to a model which *did* contain the $(3, 2, 0)$ mode, the mismatch between the fit and the signal did not have a knee where it ceased to decrease. It decreased until it reached the numerical precision of the program. This is a an important step in understanding the behavior of overtones: we know that the $(3, 2, 0)$ mode is influential in the mismatch leveling off after a knee. Although we have not yet discovered the exact way in which the $(3, 2, 0)$ QNM determines the location of knees, we know that mode is very influential.

Previous research on fitting overtones of the ringdown fit a maximum of seven overtones [3], however, there is no particular reason to stop at seven overtones. We have shown that, for these waveforms, the maximum number of overtones that can be fit is 17. The mismatch is a mathematical metric for evaluating how well a model fits the simulated data, but does not describe whether a particular model is in physical agreement with the simulation. The following subsection will introduce a more physical metric for goodness of fit and compare the times $t_0^{N,\mathcal{M}}$ generated by both methods.

2.2 Remnant mass and spin studies

Giesler et al. introduced a metric ϵ which measures the physical agreement between a fit and a NR simulation [3]. The No-Hair Theorem states that the mass M_f and dimensionless spin χ_f of the final BH completely determine the QNM frequencies. Thus, we can vary the QNM frequencies of a model by varying the model's mass and spin. For a model with N overtones and start time t_0, we minimize the mismatch $\mathcal{M}$ between the model and the signal by varying M_f and χ_f. In this work, we use `minimize` from `scipy.optimize` to perform this calculation. Then, δM_f and $\delta\chi_f$ are the differences between the simulation final mass and spin and the final mass and spin which minimize $\mathcal{M}$.

Then,

$$\epsilon = \sqrt{(\delta M_f/M)^2 + (\delta\chi_f)^2}.$$

We plot ϵ vs t_0 for CCE1 in Figure 4. Calculating ϵ is very computationally expensive, so we have only calculated ϵ as a function of t_0 for models with $N \leq 7$ so far.

Just as models with more overtones have a low mismatch at earlier times, models with more overtones have a low ϵ at earlier times. Let $t_0^{N,\epsilon}$ be the earliest time at which $\epsilon(t_0)$ reaches a local minimum. As can be seen in Figure 4, the curve has several local minima, but we choose the earliest one. This metric differs from $t_0^{N,\mathcal{M}}$ because it determines the earliest time at which a model physically matches a NR simulation. However, the two are highly correlated, especially for higher numbers of overtones (See Figure 5).

Now, let $\Delta t_0^{N,\epsilon} = t_0^{N,\epsilon} - t_0^{N-1,\epsilon}$. This is another measure of "usefulness" for each additional overtone. The greater the value of $\Delta t_0^{N,\epsilon}$ is, the more value (e.g. earlier fitting time and higher SNR) is gained by adding the Nth overtone.

Figure 6 shows $\Delta t_0^{N,\epsilon}$ vs N for all ten CCE waveforms studied. The plot shows a general downward trend in $\Delta t_0^{N,\epsilon}$, similar to Figure 2, although some CCE waveforms significantly deviate from this trend.

So far, we have defined two definitions of usefulness: $\Delta t_0^{N,\mathcal{M}}$ and $\Delta t_0^{N,\epsilon}$. Both measures show diminishing returns for each additional overtone fitted, although the decline in $\Delta t_0^{N,\epsilon}$ is less uniform.

Another method of defining the usefulness of an overtone is by how much it influences the fit overall. This was calculated by introducing a variation in frequency δ. The QNM frequencies for all but the fundamental mode were modified by a factor of $1+\delta$ for varying numbers of overtones and plotted the resultant ϵ (See Figure 7). As the number of overtones increases, the value of ϵ decreases, suggesting that each overtone does indeed improve the

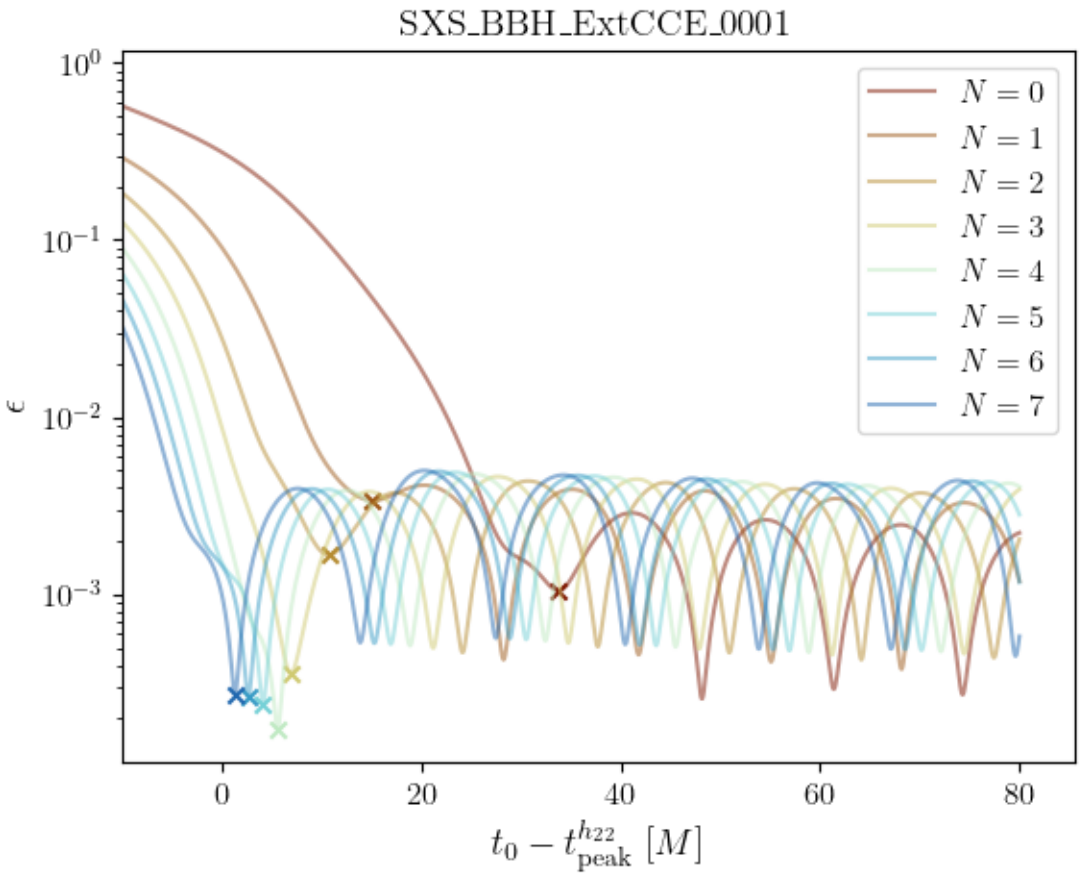

Figure 4: A plot showing the value of ϵ as a function of t_0 for CCE1. Crosses mark the location of $t_0^{N,\epsilon}$.

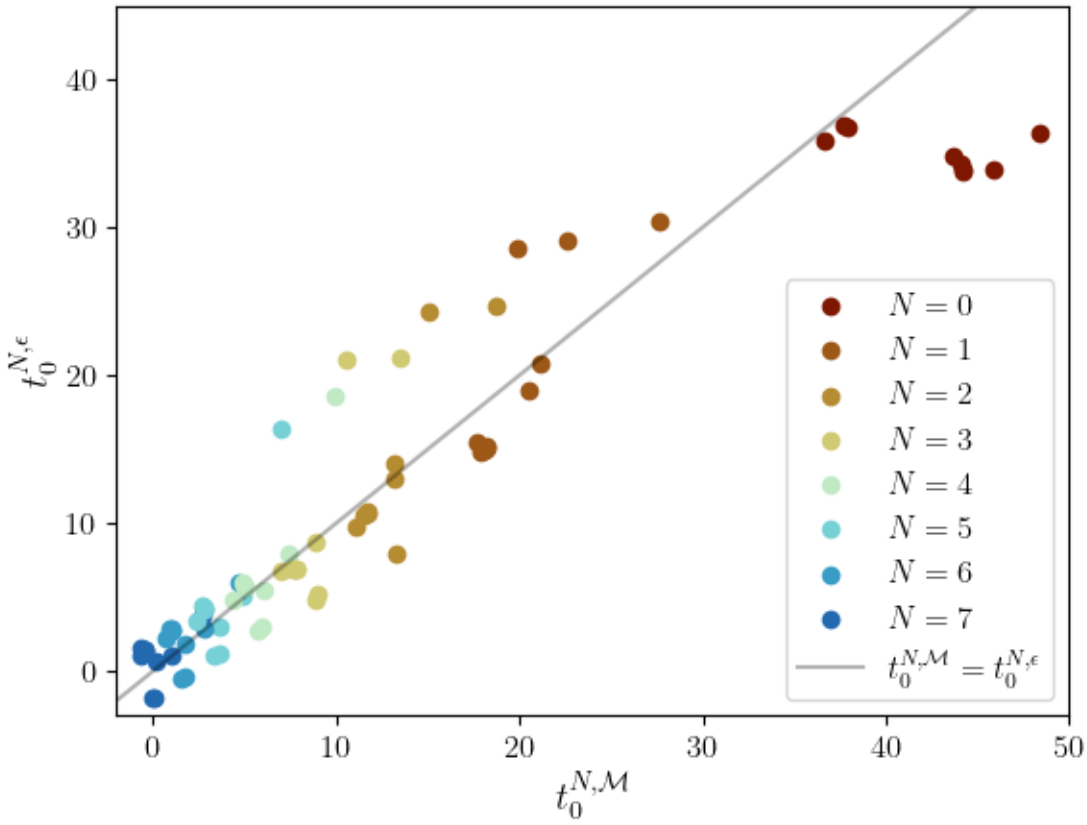

Figure 5: A plot showing $t_0^{N,\mathcal{M}}$ vs $t_0^{N,\epsilon}$ for the ten CCE waveforms used in this analysis for fits with $N \in [0, 7]$ overtones. Each point represents one fit, with color indicating the number of overtones used. The two times $t_0^{N,\mathcal{M}}$ and $t_0^{N,\epsilon}$ are correlated, especially for higher values of N.

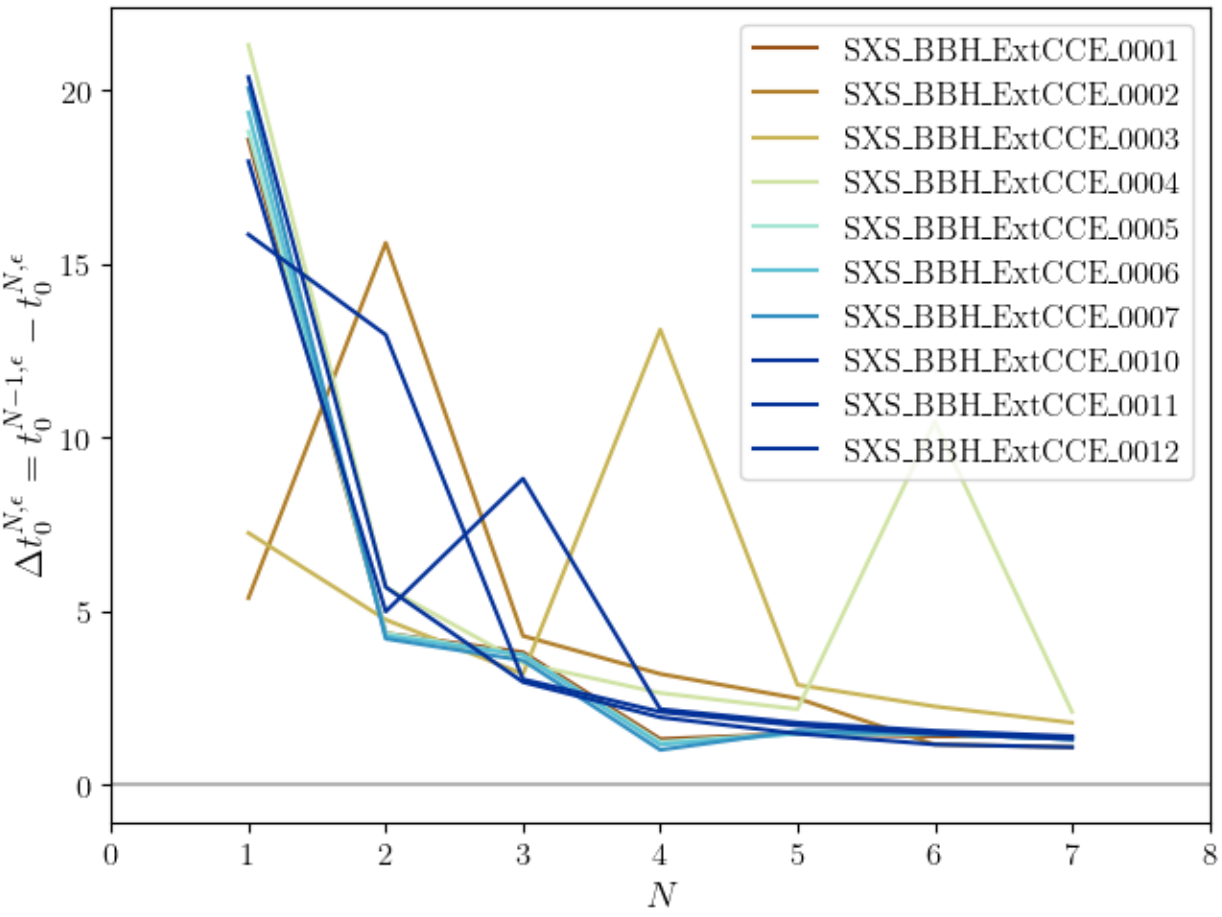

Figure 6: $\Delta t_0^{N,\epsilon}$ vs N for all ten CCE waveforms studied.

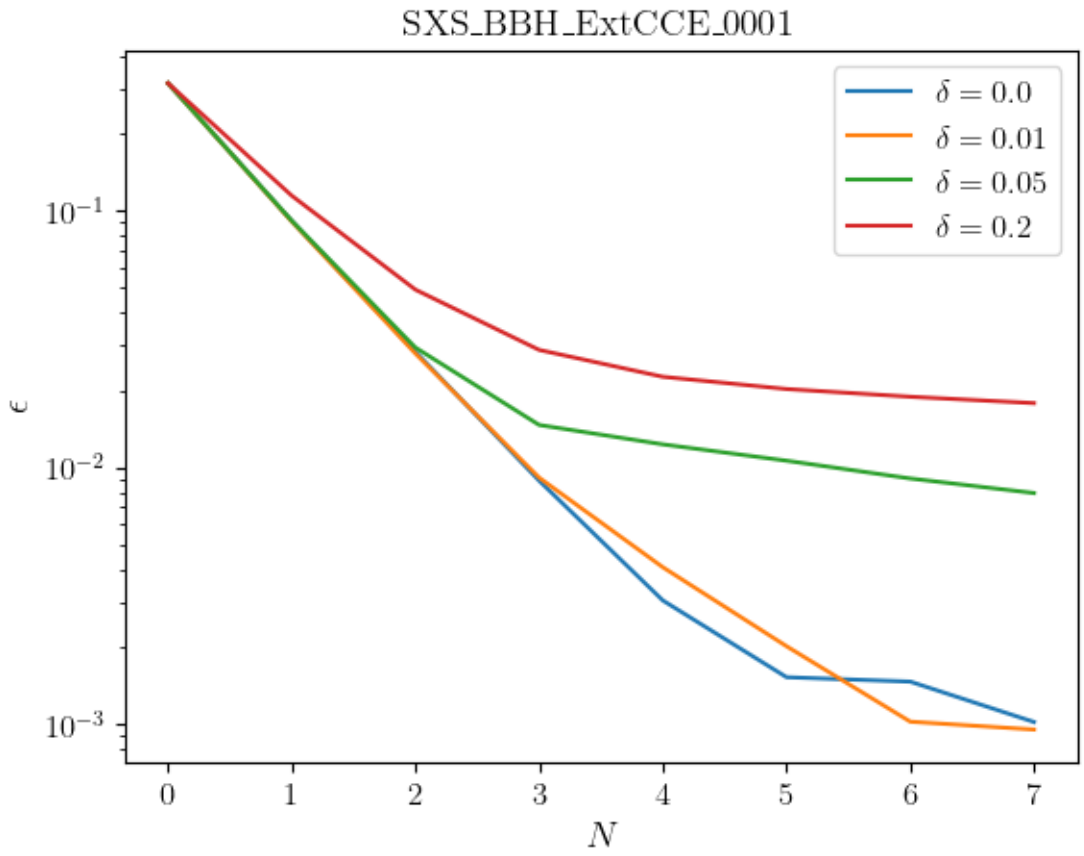

Figure 7: A plot showing the deviation ϵ from the true M_f and χ_f for different size frequency modifications δ for CCE1. The frequency of the fundamental $(2, 2, 0)$ mode was not modified in any fit. The behavior of the other CCE waveforms used in this study is similar.

match between signal and model. When frequencies are modified by a nonzero δ, the positive impact of additional overtones is less pronounced. This suggests that each overtone makes a significant contribution to the signal, and that the decrease in ϵ for higher values of N is not purely due to adding more degrees of freedom to the fit.

2.3 Amplitude recovery

We are also interested in the stability of the amplitudes of overtones for different fitting times. When a fit is performed at time t_0, it returns the amplitude of each mode at t_0. To compare amplitudes, we adjust the amplitude to be the amplitude at some time $t_{\rm ref}$. This is possible because each QNM decays at a known rate. Throughout this work, we set $t_{\rm ref} = 0 = t^{h_{22}}_{\rm peak}$. Then, we can rescale $A_{\ell mn}(t_0)$ to the reference time $t_{\rm ref}$ using the relationship

$$A_{\ell mn}(t_{\rm ref}) = A_{\ell mn}(t_0) \exp\left(\frac{t_0 - t_{\rm ref}}{\tau_{\ell mn}(M_f, \chi_f)}\right)$$

where $\tau_{\ell mn}(M_f, \chi_f)$ is the decay time of the mode [11]. $\tau_{\ell mn}$ is related to the complex frequency of the (ℓ, m, n) QNM $\omega_{\ell mn}$ by the equation

$$\tau_{\ell mn} = -\frac{1}{\mathrm{Im}[\omega_{\ell mn}]}.$$

Now that we can compare the amplitudes of QNMs fitted at different times, we measure the stability of the fitted amplitudes. Let $A^N_{\ell mn}$ be the amplitude of the (ℓ, m, n) mode in a fit with N overtones, fitted at $t_0 = t_0^{N,\mathcal{M}}$. We define

$$\Delta A^N_{\ell mn} = \frac{A^N_{\ell mn} - A^n_{\ell mn}}{A^n_{\ell mn}}.$$

The amplitude of each QNM increases rapidly with n, but $\Delta A^N_{\ell mn}$ normalizes the change in amplitude with respect to the amplitude of the nth overtone in a fit with $N = n$ overtones. By definition, $\Delta A^n_{\ell mn} = 0$. We plot $\Delta A^N_{\ell mn}$ vs N for up to seven overtones in Figure 8. It is possible to plot $\Delta A^N_{\ell mn}$ for larger numbers of overtones, but the plot becomes very large.

Figure 8 shows that the amplitudes of higher overtones are more unstable than the amplitude of lower overtones. In general, this plot also suggests that the amplitude of the nth overtone decreases as more overtones are added, although the magnitude of each decrease gets smaller. However, least-squares fitting means that

3 Future Work

All of the work I have done so far uses least-squares fits. In the coming weeks, I plan to repeat all of these analyses using Bayesian fits. In particular, I plan to introduce error bars into the measurement of fitted amplitudes. We expect that for fits performed after a QNM has decayed, that QNM's amplitude should be consistent with zero, which is not what we see in least-squares fits.

I also want to learn to run code on the cluster. Especially when calculating ϵ, these fits and calculations can be very computationally expensive, and being able to run it on dedicated computational resources would be very helpful.

4 Acknowledgement

Suggested acknowledgement: This work was supported by the National Science Foundation Research Experience for Undergraduates (NSF REU) program, the LIGO Laboratory Summer Undergraduate Research Fellowship program (NSF LIGO), and the California Institute of Technology Student-Faculty Programs.

References

[1] R. Abbott et al. "GWTC-3: Compact Binary Coalescences Observed by LIGO and Virgo during the Second Part of the Third Observing Run". In: *Phys. Rev. X* 13.4 (2023), p. 041039. DOI: 10.1103/PhysRevX.13.041039. arXiv: 2111.03606 [gr-qc].

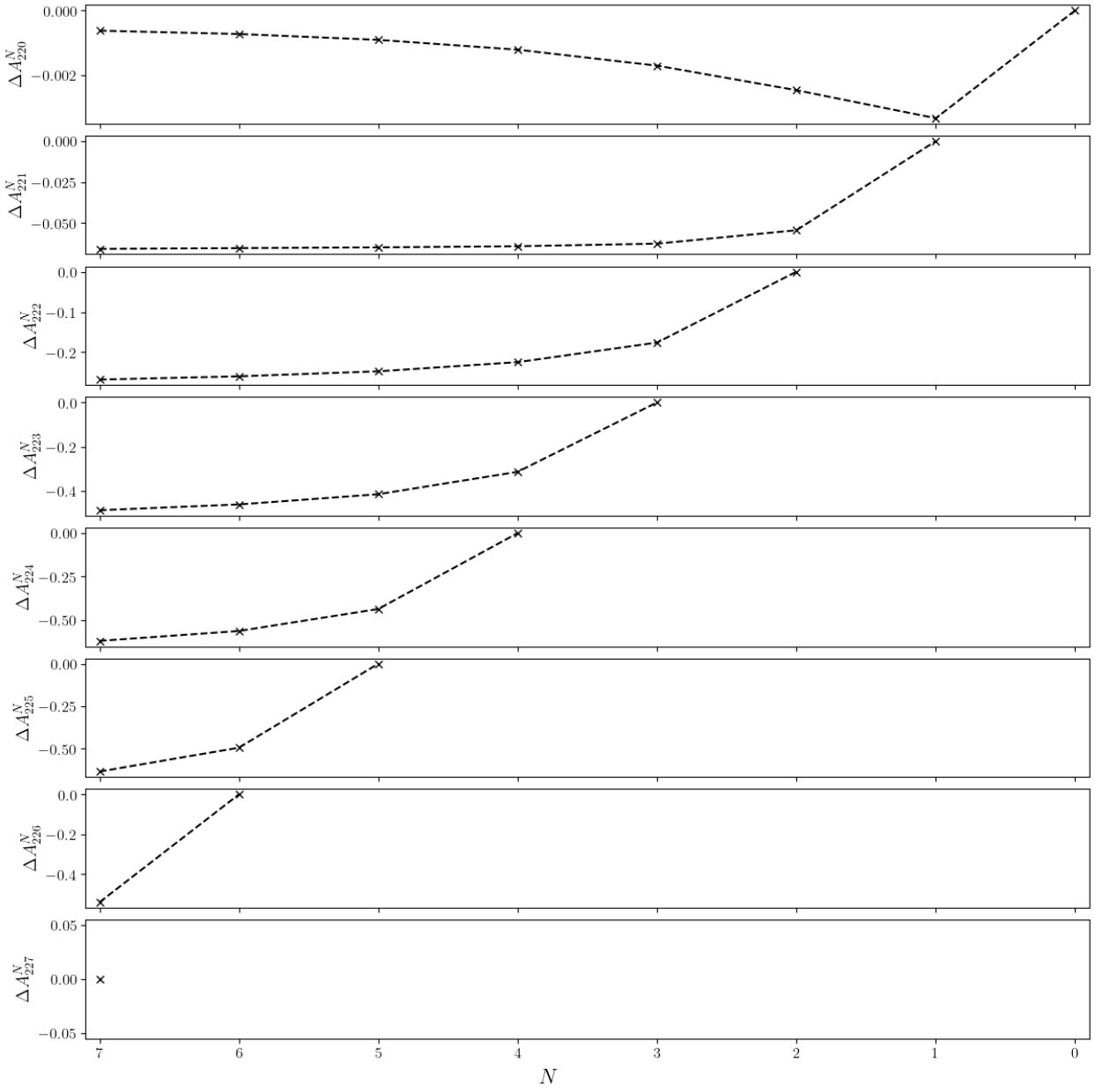

Figure 8: A plot showing the normalized change in amplitude of each QNM for a fit performed at $t_0^{N,\mathcal{M}}$, adjusted to $t_{\rm ref} = 0$, as a function of N.

[2] Teagan A. Clarke et al. "Toward a self-consistent framework for measuring black hole ringdowns". In: *Phys. Rev. D* 109.12 (2024), p. 124030. DOI: 10.1103/PhysRevD.109.124030. arXiv: 2402.02819 [gr-qc].

[3] Matthew Giesler et al. "Black Hole Ringdown: The Importance of Overtones". In: *Phys. Rev. X* 9.4 (2019), p. 041060. DOI: 10.1103/PhysRevX.9.041060. arXiv: 1903.08284 [gr-qc].

[4] Maximiliano Isi et al. "Testing the no-hair theorem with GW150914". In: *Phys. Rev. Lett.* 123.11 (2019), p. 111102. DOI: 10.1103/PhysRevLett.123.111102. arXiv: 1905.00869 [gr-qc].

[5] Gregorio Carullo, Walter Del Pozzo, and John Veitch. "Observational black hole spectroscopy: A time-domain multimode analysis of GW150914". In: *Physical Review D* 99.12 (June 2019). ISSN: 2470-0029. DOI: 10.1103/physrevd.99.123029. URL: http://dx.doi.org/10.1103/PhysRevD.99.123029.

[6] Michael Boyle et al. "The SXS Collaboration catalog of binary black hole simulations". In: *Class. Quant. Grav.* 36.19 (2019), p. 195006. DOI: 10.1088/1361-6382/ab34e2. arXiv: 1904.04831 [gr-qc].

[7] SXS Collaboration. *The Ext-CCE Waveform Database*. https://data.black-holes.org/waveforms/extcce_catalog.html.

[8] Michael Boyle et al. *scri*. Version v2022.8.10. Feb. 2024. DOI: 10.5281/zenodo.10709136. URL: https://doi.org/10.5281/zenodo.10709136.

[9] Ville Satopaa et al. "Finding a "Kneedle" in a Haystack: Detecting Knee Points in System Behavior". In: *2011 31st International Conference on Distributed Computing Systems Workshops*. 2011, pp. 166–171. DOI: 10.1109/ICDCSW.2011.20.

[10] Kevin Arvai. *kneed*. Version v0.8.5. July 2023. DOI: 10.5281/zenodo.8127224. URL: https://doi.org/10.5281/zenodo.8127224.

[11] Eliot Finch. "Black-hole Ringdown: Quasinormal Modes in Numerical-relativity Simulations and Gravitational-wave Observations". PhD thesis. University of Birmingham, 2023.